Research Article
https://doi.org/10.1631/jzus.B2600405

Dioscin suppresses renal cell carcinoma progression via targeting FABP5 to disrupt lipid metabolism and mitochondrial homeostasis

Hui WANG[1*], Yi LU[2*], Zhongyi LI[2,3*], Lifeng DING[2✉]

[1]*Department of Nursing, Sir Run Run Shaw Hospital, Zhejiang University School of Medicine, Hangzhou, 310016, China*
[2]*Department of Urology, Sir Run Run Shaw Hospital, Zhejiang University School of Medicine, Hangzhou, 310016, China.*
[3]*Department of Urology, the Second Affiliated Hospital, School of Medicine, Zhejiang University, Hangzhou 310058, China*

Abstract: Objective: This study aimed to investigate the therapeutic potential and direct molecular targets of dioscin, a natural steroid saponin, in the progression of renal cell carcinoma (RCC). Methods: The anti-tumor phenotypes of dioscin were evaluated in vitro using Cell Counting Kit-8 (CCK-8), transwell and flow cytometry assays. Biotinylated dioscin probes coupled with mass spectrometry, molecular docking, and site-directed mutagenesis were employed to identify and validate direct intracellular targets. Mitochondrial function was assessed via Seahorse OCR analysis, ROS quantification and JC-1 staining. Subcutaneous xenograft mouse models were established to verify the in vivo efficacy of dioscin. Results: Dioscin profoundly suppressed RCC cell proliferation and metastasis while inducing dose-dependent apoptosis. Mechanistically, dioscin directly bound to the T62, T63 and T76 residues of FABP5, an oncogenic lipid chaperone upregulated in RCC tissues. This targeted engagement obstructed FABP5-mediated fatty acid transport, provoking intracellular triglyceride depletion, blunted mitochondrial respiration, massive ROS accumulation, and the collapse of mitochondrial membrane potential. The systemic administration of dioscin robustly retarded tumor growth in vivo, while showing no overt hepatotoxicity, nephrotoxicity or major organ damage. Conclusions: Our findings unveiled the existence of a novel dioscin/FABP5/mitochondrial homeostasis signaling axis and demonstrated that dioscin may represent a promising and selective therapeutic candidate for restraining RCC progression.

Key words: Renal cell carcinoma; Dioscin; Fatty acid binding protein 5 (FABP5); Mitochondrial homeostasis

1 Introduction

Renal cell carcinoma (RCC) represents one of the most common and lethal malignancies within the urological system, accounting for approximately 3% to 5% of all adult systemic cancers worldwide (Rose and Kim, 2024). Among its various histological subtypes, clear cell renal cell carcinoma (ccRCC) is the most prevalent and aggressive form, characterized by a highly metabolic and vascularized phenotype (Pham and Hsu, 2025). For decades, surgical resection has remained the mainstay treatment for localized RCC; however, a substantial proportion of patients initially present with or eventually progress to metastatic or advanced disease (Chen et al., 2023; Ivanyi et al., 2024). With the introduction of targeted therapies, the therapeutic landscape for advanced RCC has evolved dramatically. Particularly anti-angiogenic multi-targeted tyrosine kinase inhibitors

✉ Lifeng DING, dinglf@zju.edu.cn
*The three authors contributed equally to this work
Lifeng DING, https://orcid.org/0009-0000-1606-1519
Hui WANG, https://orcid.org/0000-0001-5493-1247

Received June 10, 2026; Revision accepted Aug. 22, 2026;
Crosschecked xxx. xx, 20xx

(TKIs), such as sunitinib, stand as a first-line standard-of-care regimen (Bex et al., 2025). Unfortunately, despite the initial clinical benefits, the vast majority of patients inevitably develop acquired drug resistance within months, leading to treatment failure and dismal long-term survival rates (Jin et al., 2023). This clinical bottleneck underscores an urgent and compelling need to elucidate the precise molecular mechanisms driving RCC progression and to identify novel, effective therapeutic strategies that can overcome drug resistance.

Natural products and plant-derived bioactive compounds have emerged as invaluable reservoirs for novel anticancer drug discovery due to their diverse chemical structures and multi-targeted therapeutic potentials (Hao et al., 2024; Er-Rahmani et al., 2024). Dioscin, a natural steroid saponin abundantly found in various Traditional Chinese Medicine (TCM) herbs, has recently garnered substantial interest due to its potent tumor-suppressive activities (Gao et al., 2024; Wang et al., 2025). Accumulating evidence has demonstrated that dioscin exerts remarkable anti-neoplastic effects across a spectrum of human malignancies by inducing cell cycle arrest, promoting apoptosis, and suppressing tumor angiogenesis (Lai et al., 2025; Kou et al., 2026). Nevertheless, despite its documented efficacy in several solid tumors, the specific biological functions and functional downstream targets of dioscin, as well as the underlying molecular mechanisms, in the context of renal cell carcinoma remain completely unexplored, leaving a critical gap in our understanding of its therapeutic utility in urological oncology.

In the present study, we demonstrated that dioscin profoundly suppresses RCC cell proliferation and metastasis. Mechanistically, dioscin directly binds to FABP5 protein. This binding hinders FABP5-mediated fatty acid transport, thereby provoking lipid metabolism reprogramming and subsequent mitochondrial dysfunction, which ultimately suppresses renal tumor progression. Crucially, dioscin exerts a profound therapeutic effect in RCC progression in vivo. Overall, this work unveils a novel dioscin/FABP5 axis and highlights its promise as a therapeutic strategy for renal cell carcinoma.

2 Materials and methods

The study methods are extensively described in the supplementary materials and methods.

2.1 Cell lines and cell culture

The human renal cancer cell lines 769-P and ACHN were purchased from the American Type Culture Collection (ATCC). Both cell lines were cultured in RPMI 1640 medium (Gibco) supplemented with 10% (v/v) fetal bovine serum (FBS; Cellmax) and 1% (v/v) penicillin–streptomycin, and incubated at 37 °C in a humidified atmosphere with 5% CO2. All cell lines were routinely authenticated via STR profiling every six months and confirmed to be free of mycoplasma contamination throughout the experiments.

2.2 Statistical analyses

All quantitative measurements are presented as the mean ± standard deviation (SD) derived from a minimum of three independent experimental replicates. Inter-group statistical discrepancies were analyzed using GraphPad Prism software. Differences between two experimental arms were evaluated using a two-tailed Student's t-test, whereas variance across multiple experimental groups was assessed via a one-way analysis of variance (ANOVA) combined with a post-hoc Student-Newman-Keuls test. Prior to parametric analyses, the normality of data distribution was examined using the Shapiro-Wilk test, and the homogeneity of variances was verified using Levene's test; all data subjected to ANOVA met these assumptions. The statistical significance thresholds were set at a P-value <0.05.

3 Results

3.1 Dioscin suppresses RCC cell proliferation and metastasis in vitro

To elucidate the functional role of dioscin in renal cell carcinoma (RCC) progression (Fig. 1a), we first evaluated its cytotoxic effects toward malignant versus normal renal tubular epithelial cell lines HK-2. The Half maximal inhibitory concentration (IC_{50}) of dioscin in HK-2 cells was 6.09 μmol/L, substantially higher than that in 769-P (1.85 μM) and ACHN (2.04 μM) cells (Fig. 1b), indicating that dioscin preferentially inhibits malignant RCC cells over the normal renal epithelium. CCK-8 and colony formation assays demonstrated that dioscin treatment significantly reduces RCC cell viability and proliferation in a dose-dependent manner (Figs. 1c–d). Concurrently, flow cytometric analysis of cell apoptosis revealed a remarkable, dose-dependent increase in the apoptotic population following dioscin administration, indicating that dioscin triggers RCC cell apoptosis (Fig. 1e). We next investigated the impact of dioscin on the metastatic potential of RCC cells. Transwell migration assays showed that dioscin treatment significantly suppressed the migratory capacity of both RCC cell lines in a dose-dependent fashion (Fig. 1f). To further substantiate these findings, we examined the expression of epithelial-mesenchymal transition (EMT) markers. Dioscin treatment substantially upregulated the epithelial marker E-cadherin, whereas it downregulated the mesenchymal markers N-cadherin, Snail and Vimentin (Fig. 1g). Collectively, these results indicate that dioscin effectively restrains the proliferation and metastasis of RCC cells in a dose-dependent manner.

(a)

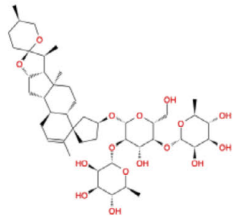

(b)

Cell line	IC50 (μM)
HK-2	6.09
769-P	1.85
ACHN	2.04

(c)

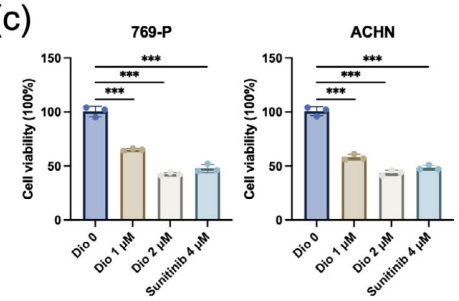

(d)

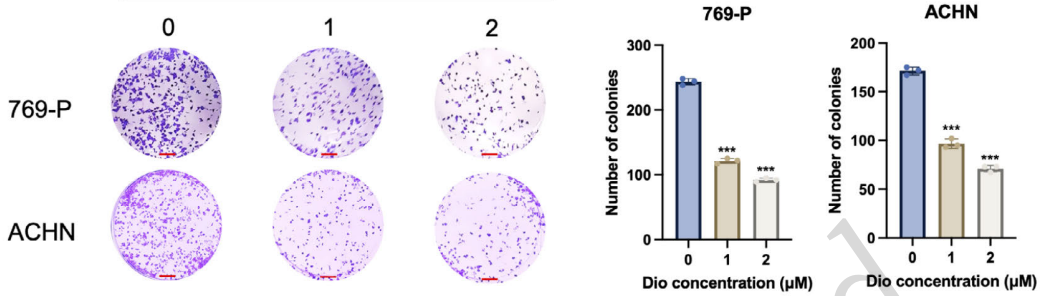

(e)

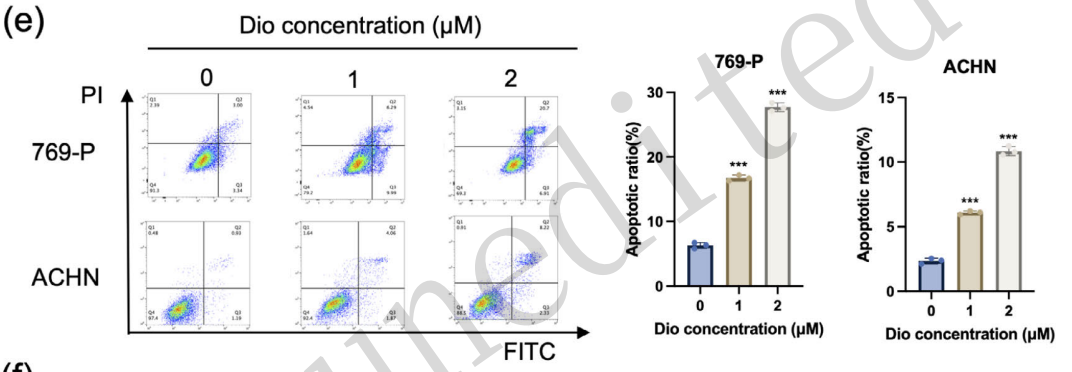

(f)

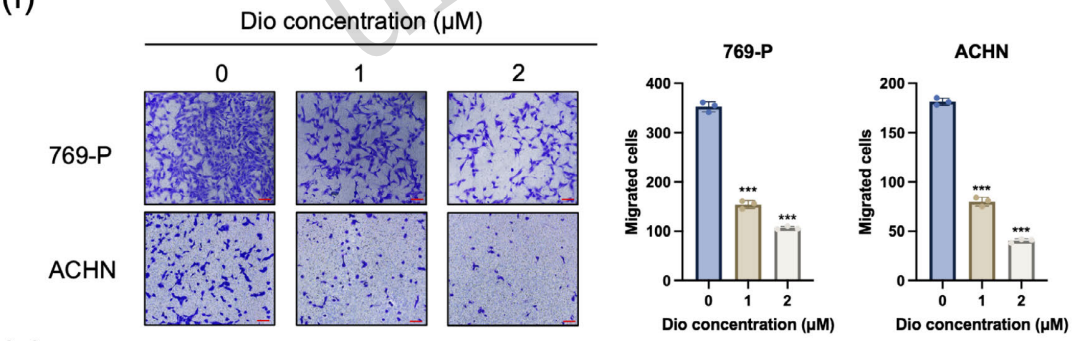

(g)

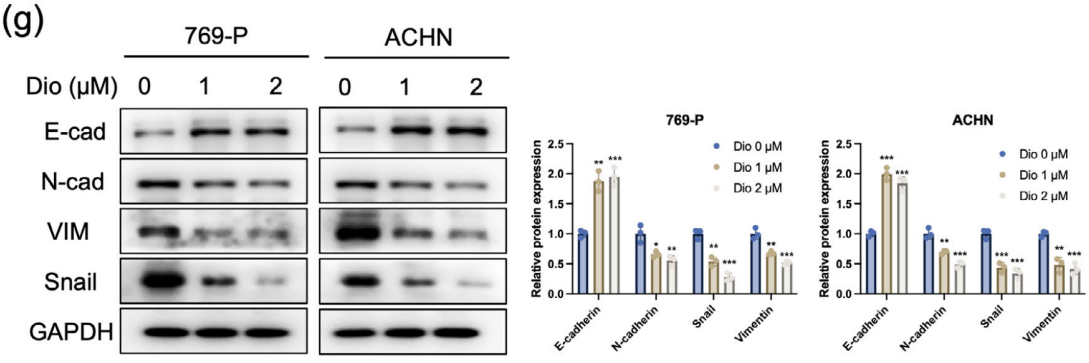

Fig. 1 Dioscin suppresses RCC cell proliferation and metastasis in vitro. (a) Schematic diagram showing the molecular structure of dioscin. (b) Table showing the detailed IC50 information for HK-2, 769-P and ACHN cells. (c) CCK-8 assays showing the cell viability of 769-P and ACHN cells under dioscin treatment, with sunitinib as a positive control (n=3). (d) Colony formation assays showing the cell viability of 769-P and ACHN cells under dioscin treatment (n=3); scale bars, 5 mm. (e) Apoptosis assay showing the apoptotic ratio of 769-P and ACHN cells under dioscin treatment (n=3). (f) Transwell assays showing the metastatic ability of 769-P and ACHN cells under dioscin treatment (n=3); scale bars, 20 μm. (g) Western blot assays showing the EMT markers expression in 769-P and ACHN cells under dioscin treatment (n=3). Data are presented as mean ± SD; one-way ANOVA was used for (c, d, e, f, g). ***P < 0.001.

3.2 Dioscin directly binds to the FABP5 protein

To identify the downstream molecular targets through which dioscin exerts its anti-tumor effects in RCC, we synthesized a biotinylated dioscin probe (biotin-dioscin) based on its chemical structure and performed biotin-avidin pulldown assays coupled with mass spectrometry (MS) analysis. To identify specific binding partners of dioscin and minimize non-specific proteomic noise, raw MS datasets were subjected to a background-subtraction filter, whereby proteins exhibiting more than 3 unique peptides in the biotin control group were excluded. Within this cleared specific candidate pool, FABP5 ranked first based on the unique peptide count and sequence coverage analysis (Figs. 2a–b). Consequently, FABP5 was selected for subsequent mechanistic investigation. The physical interaction between dioscin and FABP5 was further validated by western blot analysis following biotin pulldown assays (Fig. 2c). To prove the direct interaction between dioscin and FABP5, a microscale thermophoresis (MST) assay was conducted. The results confirmed that dioscin directly bound to GFP-FABP5 with a favorable dissociation constant (KD) of 95.15 μM (Fig. 2d). Furthermore, molecular docking simulations were performed based on the established crystal structure of FABP5 (PDB ID: 4LKP), revealing a high-affinity binding pocket for dioscin with a robust binding score of -8.8 kcal/mol (Fig. 2e). Notably, docking analysis indicated that the hydroxyl groups of dioscin form critical hydrogen bonds with the T62, T63 and T76 residues of FABP5. To validate these crucial binding sites, we constructed a mutant FABP5 plasmid (FABP5-mut) carrying T62A, T63A and T76A substitutions. Biotin pulldown assays demonstrated that while biotin-dioscin efficiently pulled down wild-type (WT) FABP5, it failed to interact with FABP5-Mut, confirming that the T62, T63 and T76 residues are indispensable for mediating the dioscin-FABP5 interaction (Fig. 2f). Additionally, cellular thermal shift assays (CETSA) revealed that dioscin treatment substantially enhanced the thermal stability of FABP5 protein (Fig. 2g). Taken together, these data demonstrate that dioscin directly and physically binds to FABP5.

(a)

Protein name	Unique peptide	Sequence coverage
FABP5	26	36%
HNRNPR	20	16%
S100A8	18	22%
HSP90AB1	17	15%
.....	.....	.....

(b)

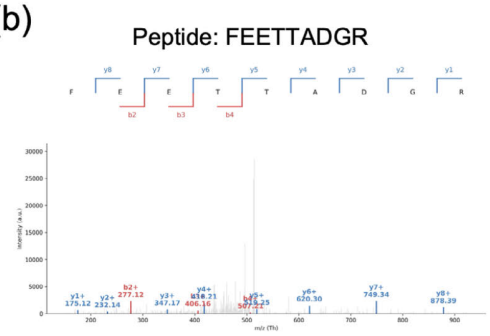

(c)

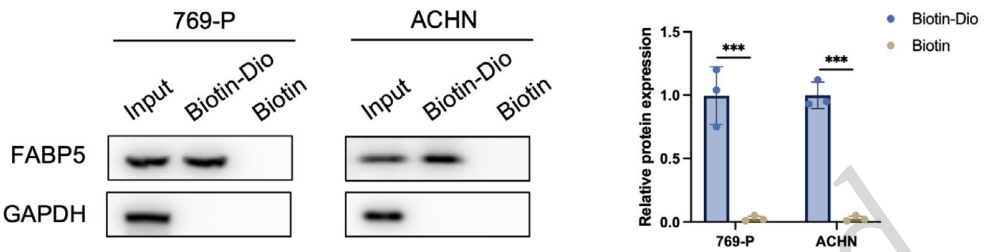

(d)

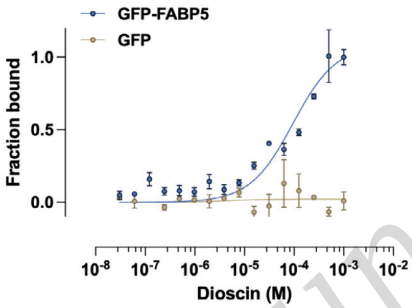

(e)

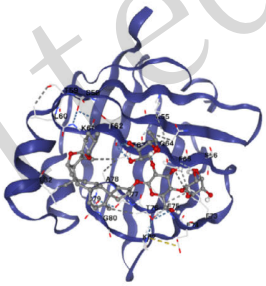

Binding affinity: -8.8 kcal/mol

(f)

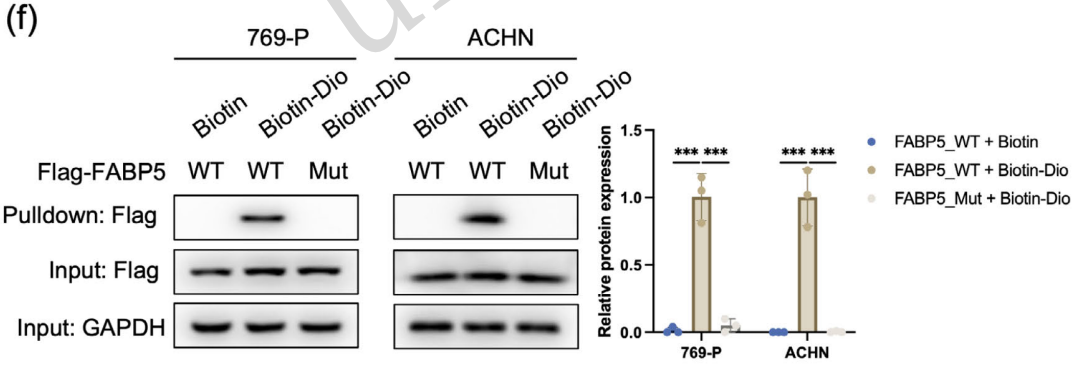

(g)

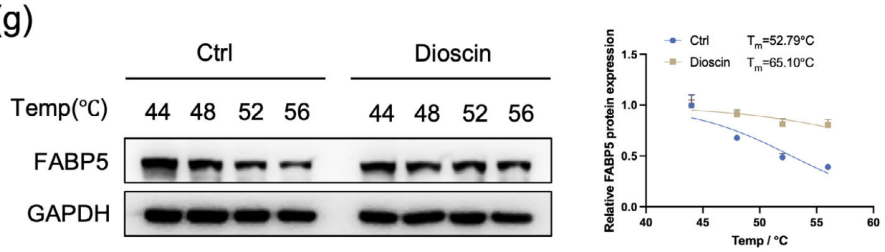

Fig. 2 Dioscin directly binds to the FABP5 protein. (a) Table showing the top 4 dioscin-binding proteins according to mass spectrometry. (b) Mass spectrometry showing the typical peptide of FABP5 according to mass spectrometry. (c) WB assays showing the binding capacity between FABP5 and dioscin in 769-P and ACHN cells (n = 3). (d) MST assay showing the binding capacity between FABP5 and dioscin (n=3). (e) Molecular docking assay showing the binding model between FABP5 and dioscin. (f) WB assays showing the binding capacity between dioscin to FABP5 wild type or mutant in 769-P and ACHN cells (n=3). (g) CETSA assay showing the FABP5 protein stability with or without dioscin (n=3). Data are presented as mean ± SD. One-way ANOVA was used for (f). ***P < 0.001.

3.3 FABP5 facilitates the malignant progression of RCC cells

To ascertain the clinical significance and biological role of FABP5 in RCC, we first analyzed its expression profiles across RCC subtypes using public datasets. In the TCGA-KIRC (clear cell RCC) cohort, FABP5 mRNA was significantly elevated in tumor tissues compared with adjacent normal tissues (Fig. 3a). Consistently, FABP5 mRNA was also significantly upregulated in the TCGA-KIRP (papillary RCC) cohort (Fig. S1a). At the protein level, CPTAC analysis confirmed increased FABP5 protein abundance in ccRCC tumor versus normal tissues (Fig. 3b). Kaplan-Meier survival analysis in the KIRC cohort demonstrated that high FABP5 expression correlated with significantly poorer overall survival (Fig. 3c), whereas no significant difference was observed in the KIRP cohort, likely due to the smaller sample size in this dataset (Fig. S1b). Collectively, these data indicated that FABP5 is aberrantly overexpressed across RCC subtypes and may function as an oncogene in RCC.

To experimentally define the biological role of FABP5, we performed both loss- and gain-of-function studies in RCC cells. CCK-8 and colony formation assays demonstrated that FABP5 depletion significantly suppressed RCC cell proliferation, while FABP5 overexpression significantly accelerated it (Figs. 3d–g). Consistently, transwell migration assays showed a marked impairment of cell motility upon FABP5 knockdown (Fig. 3h), while it was enhanced by FABP5 overexpression (Fig. 3i). These complementary loss- and gain-of-function findings collectively establish FABP5 as a bona fide pro-tumorigenic factor that promotes the proliferation and metastatic capacity of RCC cells.

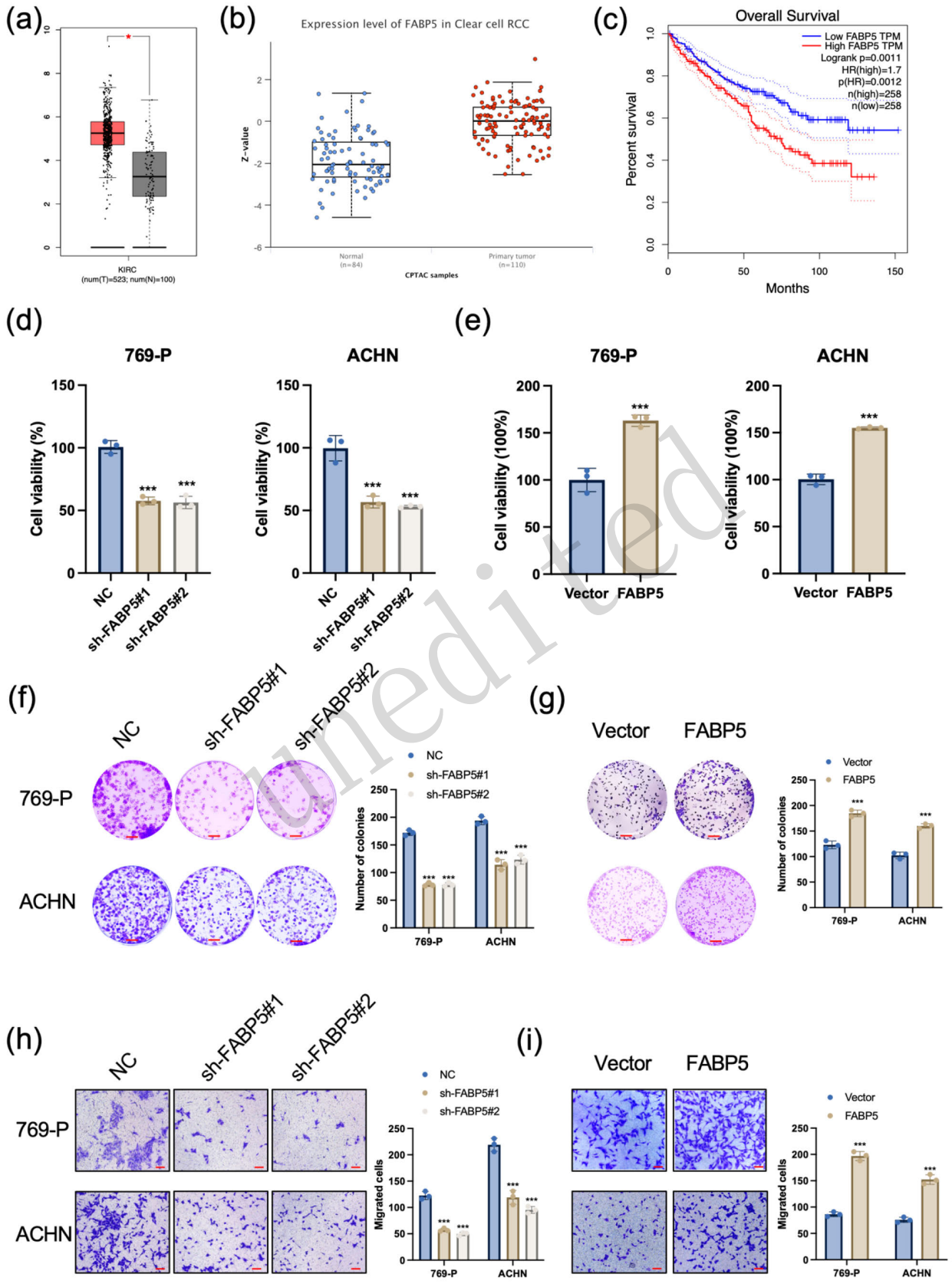

Fig. 3 FABP5 facilitates the malignant progression of RCC cells. (a) GEPIA analysis of TCGA-KIRC RNA-sequencing

data showing FABP5 mRNA expression in RCC tumor tissues (n=523) versus normal kidney tissues (n=100). (b) UALCAN analysis of CPTAC proteomic data showing FABP5 protein expression in ccRCC tumor tissues (n=110) versus normal kidney tissues (n=84). (c) K-M survival analysis showing the overall survival in ccRCC patient with FABP5 high expression or low expression. (d) CCK-8 assays showing the cell viability of 769-P and ACHN cells with FABP5 knockdown (n=3). (e) CCK-8 assays showing the cell viability of 769-P and ACHN cells with FABP5 overexpression (n=3). (f) Colony formation assays showing the cell viability of 769-P and ACHN cells with FABP5 knockdown (n=3); scale bars, 5 mm. (g) Colony formation assays showing the cell viability of 769-P and ACHN cells with FABP5 overexpression (n=3); scale bars, 5 mm. (h) Transwell assays showing the metastatic ability of 769-P and ACHN cells with FABP5 knockdown (n=3); scale bars, 20 μm. (i) Transwell assays showing the metastatic ability of 769-P and ACHN cells with FABP5 overexpression (n=3); scale bars, 20 μm. Data are presented as mean ± SD; two-tailed unpaired t-test for (e, g, i), one-way ANOVA was used for (d, f, h); ***p < 0.001.

3.4 Dioscin restrains RCC malignancy in an FABP5-dependent manner

Given that FABP5 acts as a potent driver of RCC proliferation and metastasis, we next investigated whether dioscin exerts its tumor-suppressive functions by targeting FABP5. Rescue experiments were conducted by overexpressing FABP5 in dioscin-treated RCC cells. CCK-8 and colony formation assays revealed that the profound inhibition of cell proliferation induced by dioscin was substantially rescued by FABP5 overexpression (Figs. 4a–b). Similarly, transwell migration assays demonstrated that FABP5 overexpression effectively counteracted the dioscin-mediated suppression of RCC cell motility (Fig. 4c). Collectively, these results imply that dioscin impedes the malignant phenotypes of RCC cells predominantly through the deregulation of FABP5.

To further test the functional dependency of dioscin on FABP5, we examined the effect of dioscin treatment in the context of FABP5 depletion. In FABP5-knockdown cells, dioscin treatment produced little additional effects on cell proliferation (Figs. 4d–e) and migration (Fig. 4f), indicating that the anti-tumor activity of dioscin was largely attenuated when FABP5 expression was already suppressed. Collectively, these bidirectional rescue experiments demonstrate that FABP5 is the critical mediator through which dioscin exerts its anti-tumor effects in RCC cells.

To further determine whether the physical binding of dioscin to FABP5 is functionally required for its anti-tumor activity, we performed structure-function rescue experiments. In the sh-FABP5 background, 769-P cells were reconstituted with either FABP5-WT or the binding-defective FABP5-Mut, followed by dioscin treatment. In cells expressing FABP5-WT, dioscin treatment significantly suppressed cell proliferation and migration, recapitulating its effects in parental cells. In contrast, cells expressing FABP5-Mut were largely refractory to dioscin treatment, showing no significant reduction in proliferation or migration. Importantly, FABP5-Mut retained a pro-tumorigenic activity comparable to FABP5-WT in the absence of dioscin (Figs. S2a, b), confirming that the triple mutation does not impair FABP5 oncogenic function but specifically abolishes its capacity to mediate the pharmacological effects of dioscin. These data provide direct functional evidence that the T62/T63/T76 binding pocket is indispensable for the anti-tumor action of dioscin.

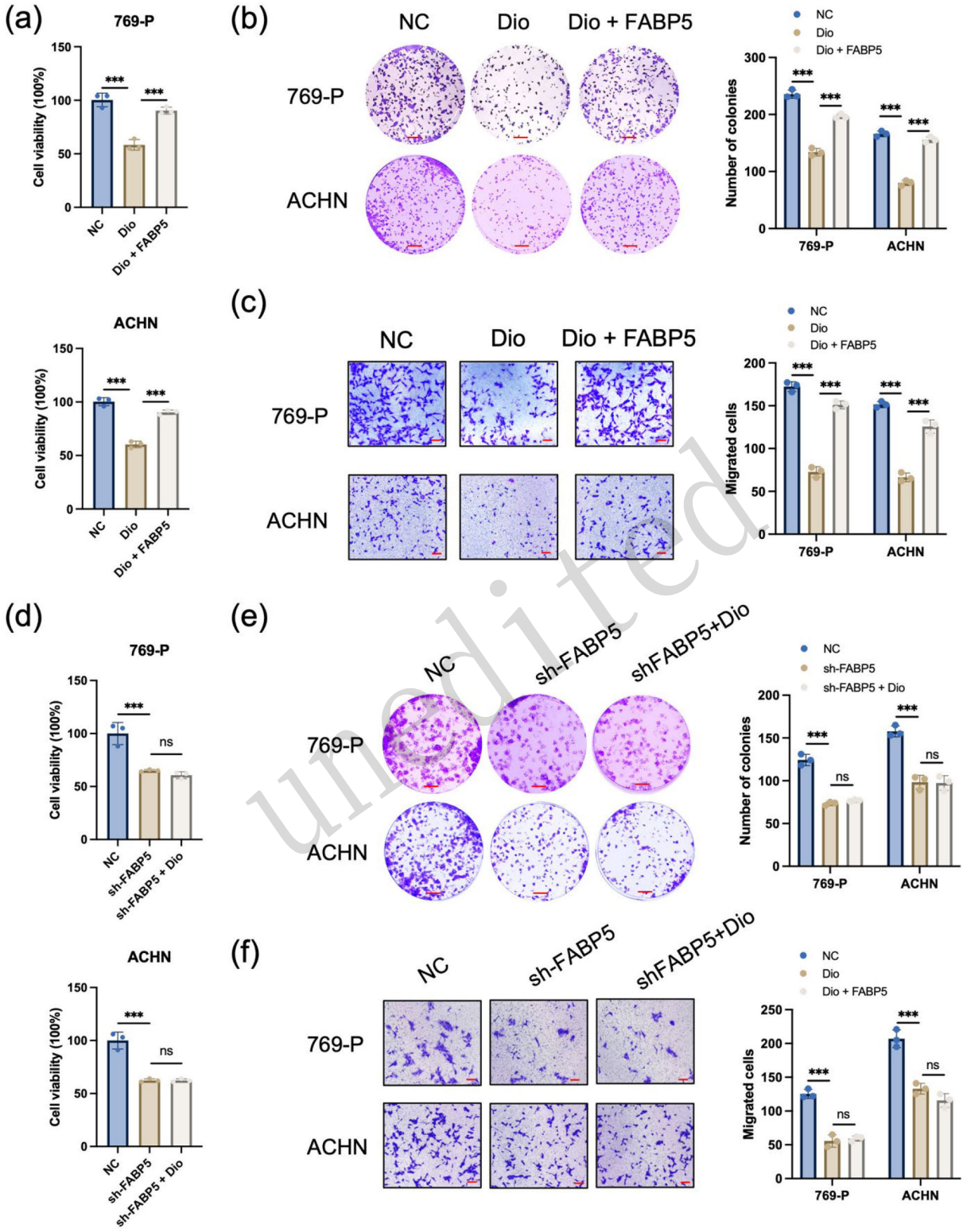

Fig. 4 Dioscin restrains RCC malignancy in an FABP5-dependent manner. (a) CCK-8 assays showing the cell viability of dioscin-treated 769-P and ACHN cells with FABP5 overexpression (n=3). (b) Colony formation assays showing the cell viability of dioscin-treated 769-P and ACHN cells with FABP5 overexpression (n=3); scale bars, 5 mm. (c) Transwell assays showing the metastatic ability of dioscin-treated 769-P and ACHN cells with FABP5 overexpression (n=3); scale bars, 20 μm. (d) CCK-8 assays showing the cell viability of FABP5 knockdown RCC cells with dioscin

treatment (n=3). (e) Colony formation assays showing the cell viability of FABP5 knockdown RCC cells with dioscin treatment (n=3); scale bars, 5 mm. (f) Transwell assays showing the metastatic ability of FABP5 knockdown RCC cells with dioscin treatment (n=3); scale bars, 20 μm. Data are presented as mean ± SD; one-way ANOVA was used for (a–f). ***p < 0.001, ns, no significance.

3.5 The dioscin/FABP5 axis impairs mitochondrial homeostasis by disrupting lipid metabolism in RCC

As a crucial intracellular chaperone, FABP5 plays a fundamental role in binding and transporting long-chain fatty acids to specific cellular compartments, thereby fuel-preferring metabolic pathways and maintaining mitochondrial lipid homeostasis (M. Li et al., 2025; Wu et al., 2025). Given that mitochondria serve as the primary destination for fatty acid β-oxidation (FAO) to support tumor energetic demands (Yu et al., 2025; D. Li et al., 2025), we reasoned that the dioscin/FABP5 interaction might disrupt the lipid architecture and consequently impair mitochondrial stability. We initially observed that dioscin treatment led to a prominent reduction in intracellular triglyceride (TG) levels in RCC cells, a phenotype that was markedly rescued by the ectopic overexpression of FABP5 (Fig. 5a). To explore whether this lipid depletion extended to mitochondrial bioenergetics, we measured the oxygen consumption rate (OCR) utilizing a Seahorse XF analyzer. Dioscin treatment severely blunted mitochondrial respiration, whereas FABP5 overexpression significantly restored the maximal respiration rates (Figs. 5b–d). Notably, these OCR measurements were performed with strict normalization: cells were counted and seeded at equal viable cell densities, with metabolic recording initiated only after complete cell attachment. This experimental design ensured that the observed respiratory deficits reflect genuine mitochondrial dysfunction rather than reduced cell number or viability. Because a deficit in mitochondrial electron transport chain efficiency often provokes a surge in electron leakage, we next quantified intracellular reactive oxygen species (ROS) levels. Flow cytometry assays showed that dioscin administration dramatically induced ROS accumulation, which was drastically attenuated upon FABP5 overexpression (Fig. 5e). Furthermore, JC-1 staining demonstrated that dioscin caused a substantial dissipation of the mitochondrial membrane potential (MMP), which was effectively rescued by FABP5 restoration (Fig. 5f). Together, these lines of evidence demonstrate that the dioscin/FABP5 axis induces a profound collapse of mitochondrial homeostasis via the deregulation of lipid metabolism, ultimately suppressing RCC progression.

To corroborate the functional relevance of the dioscin-FABP5 binding in the metabolic context, we performed OCR analysis in the sh-FABP5/OE-WT/OE-Mut reconstitution system. Consistent with the proliferation and migration data, dioscin treatment markedly suppressed mitochondrial respiration in FABP5-WT cells, whereas FABP5-Mut cells were resistant to dioscin-induced respiratory inhibition (Figs. S2c–d). This result confirms that the metabolic collapse triggered by dioscin is a direct consequence of its physical engagement with the T62/T63/T76 pocket of FABP5.

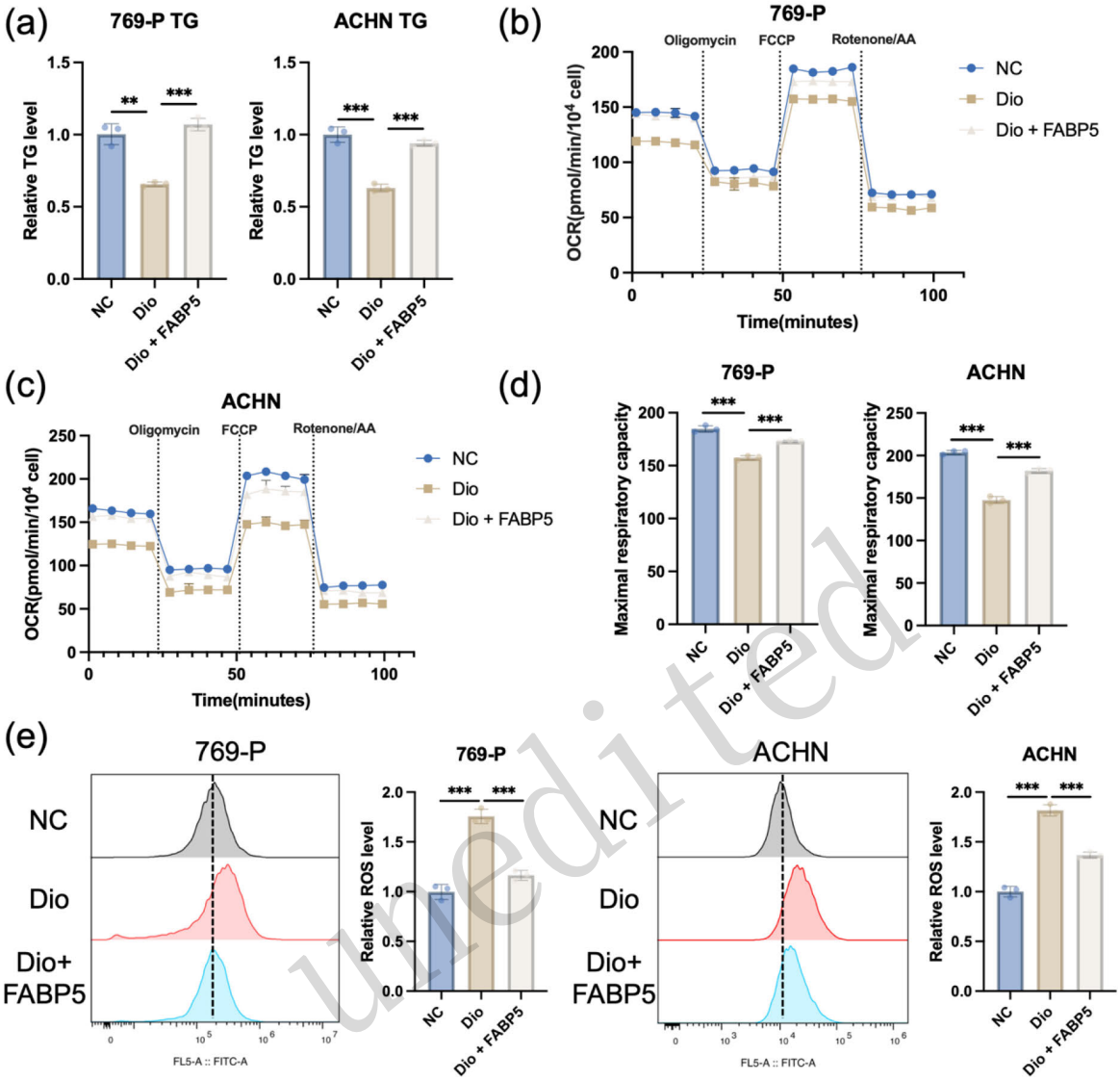
(a)
769-P TG
ACHN TG
Relative TG level
NC
Dio
Dio + FABP5
(b)
769-P
Oligomycin
FCCP
Rotenone/AA
OCR(pmol/min/10^4 cell)
Time(minutes)
(c)
ACHN
(d)
Maximal respiratory capacity
(e)
Relative ROS level
FL5-A :: FITC-A
(f)
Monomers
Aggravates
Merge

Fig. 5 The dioscin/FABP5 axis impairs mitochondrial homeostasis by disrupting lipid metabolism in RCC. (a) Intracellular triglyceride was detected in dioscin-treated 769-P and ACHN cells with FABP5 overexpression (n=3). (b-d) OCR assays showing the mitochondrial respiratory of dioscin-treated 769-P and ACHN cells with FABP5 overexpression (n=3). (e) Flow cytometry assays showing the ROS level of dioscin-treated 769-P and ACHN cells with FABP5 overexpression (n=3). (f) Mitochondrial membrane potential assays showing the MMP in dioscin-treated 769-P and ACHN cells with FABP5 overexpression (n=3); scale bar, 50 μm. Data are presented as mean ± SD; one-way ANOVA was used for (a, d, e). **p < 0.01, ***p < 0.001.

3.6 Dioscin impedes RCC progression in vivo with a favorable safety profile

To evaluate the in vivo therapeutic efficacy of dioscin and benchmark it against the standard-of-care agent, we established a 769-P subcutaneous xenograft mouse model with five treatment arms: vehicle control, three graded doses of dioscin (20, 40 and 60 mg/kg, oral gavage daily), and sunitinib (25 mg/kg, oral gavage daily) as a positive control (Fig. 6a). Dioscin treatment dose-dependently restricted tumor growth, with the 20 mg/kg dose producing a moderate reduction in tumor volume and weight, while the 40 and 60 mg/kg doses elicited progressively greater tumor suppression (Figs. 6b–d). Notably, dioscin at 60 mg/kg outperformed sunitinib, achieving significantly greater tumor growth inhibition than the current first-line targeted therapy (Figs. 6b–d).

To assess the translational safety of dioscin, we first monitored body weight changes throughout the treatment course. No significant body weight loss was observed in any of the three dioscin-treated groups compared with the control group (Fig. 6e), suggesting the absence of overt systemic toxicity. We next performed the histopathological examination of major organs (heart, liver, spleen, lung, and kidney) by H&E staining in the NC and dioscin 60 mg/kg groups. No apparent histomorphological abnormalities, inflammatory infiltration or tissue necrosis was detected in any organ examined (Fig. 6f). Furthermore, serum biochemical analysis revealed no significant differences in ALT, AST or creatinine levels between the NC and dioscin 60 mg/kg groups (Figs. 6g-i), indicating that high-dose dioscin treatment did not compromise hepatic or renal function.

To determine whether dioscin suppresses RCC tumor growth in vivo in an FABP5-dependent manner, we performed an in vivo rescue experiment (Fig. S3a). ACHN cells stably expressing vector control or OE-FABP5 were inoculated subcutaneously into nude mice, which were then treated with vehicle or dioscin (20 mg/kg). Consistent with the in vitro findings, OE-FABP5 significantly accelerated tumor growth compared with the vector control group. Dioscin treatment markedly suppressed tumor growth in the NC group; however, this anti-tumor effect was substantially attenuated in the OE-FABP5 group, with tumor volumes and weights partially restored toward control levels (Figs. S3b-d). These in vivo rescue data provide organism-level confirmation that FABP5 is a functional mediator of the anti-tumor activity of dioscin.

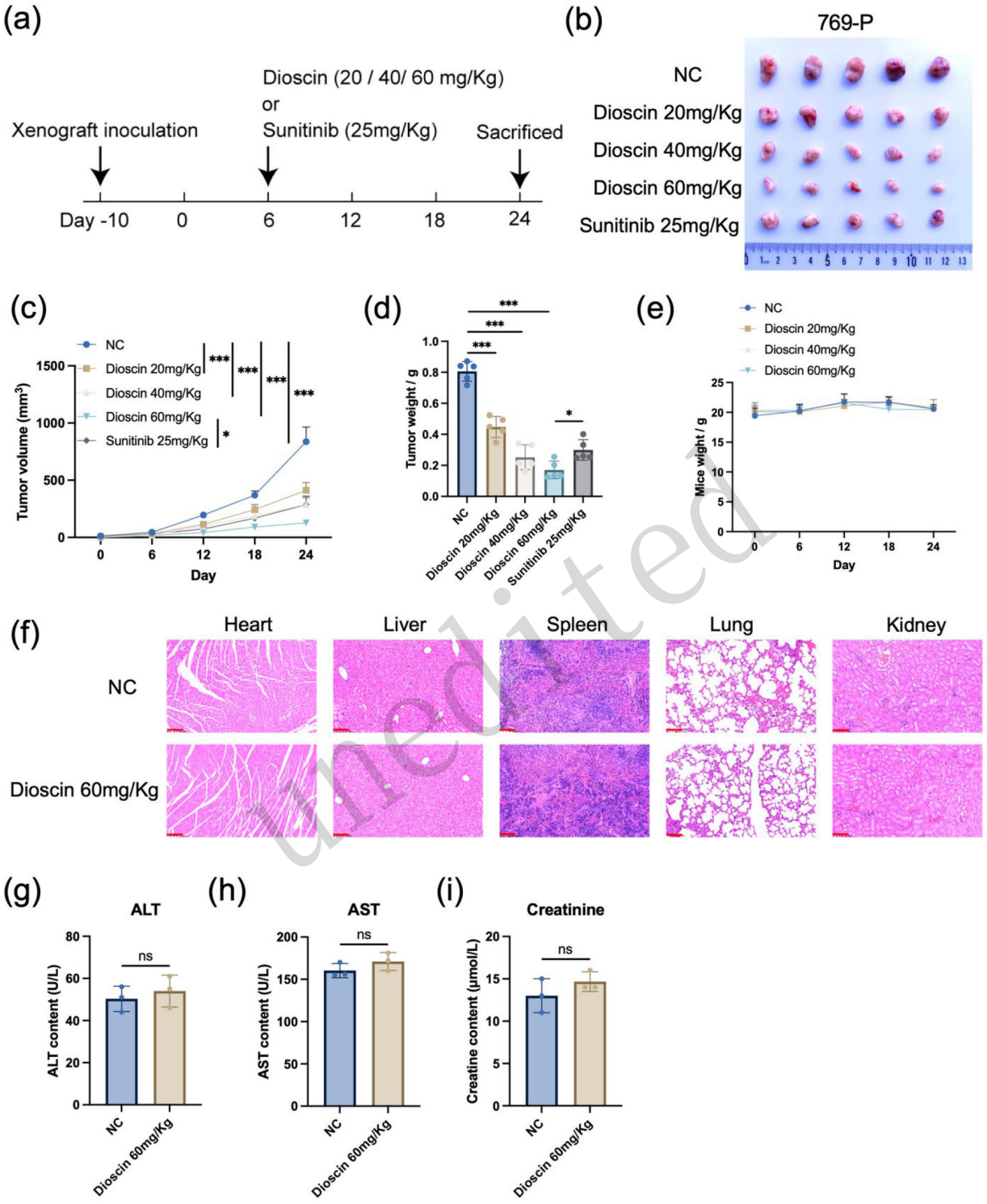

Fig. 6 Dioscin impedes RCC progression in vivo with a favorable safety profile. (a) Schematic diagram showing the experimental design of the animal study. 769-P xenograft-bearing mice were randomized into five groups (n=5 per group): NC, dioscin (20 mg/kg), dioscin (40 mg/kg), dioscin (60 mg/kg), and sunitinib (25 mg/kg), all administered via oral gavage daily. (b-d) Images (b), volumes (c) and weights (d) of indicated 769-P xenografts treated with dioscin or sunitinib (n=5). (e) Body weight changes of mice in each group throughout the treatment period. (f) Representative H&E staining images of heart, liver, spleen, lung, and kidney tissues from the NC and dioscin 60 mg/kg groups, scale

bar, 100 μm. (g-i) Serum levels of ALT, AST and creatinine in the NC and dioscin 60 mg/kg groups. Data are presented as mean ± SD; one-way ANOVA was used for (c, d), two-tailed unpaired t-test for (g-i), *p < 0.05, ***p < 0.001, ns, no significance.

4 Discussion

Natural products, particularly herbal steroidal saponins, have increasingly captured scholars' attention in urological oncology due to their structural diversity and multi-channeled anti-neoplastic activities (Song et al., 2026). Dioscin has been documented to exert inhibitory effects on several solid tumors by inducing cell cycle arrest and activating apoptotic cascades (Wang et al., 2024; Bai et al., 2024). However, its specific phenotypic impact on renal malignancies has not been explored. Our in vitro data explicitly filled this gap, revealing that dioscin markedly reduces the viability and colony formation capability of both 769-P and ACHN cells in a dose-dependent manner. This loss of viability was accompanied by a pronounced increase in the apoptotic cell population. Furthermore, dioscin suppressed RCC cell migration by epithelial marker E-cadherin, whereas it concurrently downregulated the mesenchymal markers. These phenotypic assessments establish dioscin as a potent anti-tumor agent against RCC, providing a solid biological foundation for its further mechanistic dissection.

Identifying the direct targets of natural compound monomers requires both structural accessibility and high specificity (Er-Rahmani et al., 2024). In this study, we successfully bypassed these limitations by synthesizing a biotin-dioscin probe, which, when coupled with high-throughput mass spectrometry, identified FABP5 as the premier high-affinity interacting partner of dioscin. Our validation through western blot, molecular docking and CETSA collectively confirmed this physical interaction. Crucially, rather than relying solely on computational docking predictions, we extended our investigation to mutation analysis. By substituting the predicted hydrogen-bonding residues (T62A, T63A, T76A), we observed a complete ablation of the binding affinity of dioscin to the FABP5-mut protein. This structural validation provides definitive proof that these three specific threonine residues are the absolute gatekeepers mediating the drug-protein complex, shifting our understanding of dioscin from a phenomenological compound to a target-directed monomer.

FABP5 functions canonically as a critical intracellular chaperone that delivers long-chain fatty acids to metabolic hubs, notably the mitochondria for β-oxidation, to fuel the heavy energetic demands of malignant cells (George Warren et al., 2023; Kou et al., 2025). Public dataset analyses from TCGA and CPTAC alongside our survival evaluations confirmed that FABP5 is aberrantly overexpressed in RCC and marks a dismal prognosis, framing it as an active oncogenic driver. Our functional rescue experiments successfully linked the tumor-suppressive phenotypes of dioscin directly to FABP5 deregulation. More importantly, we connected this target inhibition to its metabolic consequences. By demonstrating that dioscin significantly drains intracellular triglycerides and blunts mitochondrial respiration, both of which were reversed by FABP5 overexpression, we showed that the dioscin/FABP5 interaction effectively chokes the fatty acid utilization pathways of RCC cells. This metabolic bottleneck directly manifested as a severe bioenergetic crisis, marked by massive ROS accumulation and a profound drop in the mitochondrial membrane potential. These results tightly weave FABP5 into our dioscin-mediated pathway, demonstrating that the dioscin/FABP5 axis acts as a metabolic switch that collapses mitochondrial homeostasis by dismantling the lipid utilization network necessary for RCC survival.

It is important to acknowledge certain limitations of our mechanistic exploration. Due to technical constraints, our study infers the disruption of fatty acid oxidation (FAO) primarily through the observed depletion of intracellular lipids and the concurrent collapse of overall mitochondrial respiration. While this aligns well with the canonical role of FABP5 in shuttling lipid substrates to mitochondria for FAO, direct validation is lacking. Future investigations employing precise exogenous lipid rescue models, Seahorse XF Palmitate Oxidation Stress Tests, or stable isotope tracing are warranted to definitively establish the causal metabolic flux linking dioscin-induced FABP5 inhibition to mitochondrial catastrophe. Additionally, while the

subcutaneous xenograft model employed herein is well-suited for target validation and genetic rescue studies, orthotopic and experimental metastasis models would provide greater clinical relevance for evaluating the effects of dioscin on the RCC tumor microenvironment and metastatic dissemination. These next steps are warranted in the translational development of dioscin.

5 Conclusions

Our study clarifies a novel target-directed mechanism where dioscin directly engages the T62/T63/T76 binding pocket of FABP5, successfully interrupting its fatty acid transport capacity. This binding initiates a catastrophic lipid metabolic disruption that impairs mitochondrial respiration, triggers a ROS burst, and shatters mitochondrial membrane potential stability to suppress RCC progression. Overall, this framework provides novel mechanistic insights into natural pharmacology and highlights dioscin as a promising selective therapeutic strategy for RCC.

Data availability statement

The data that support the findings of this study are available from the corresponding author upon reasonable request.

Acknowledgments

This project was funded by Zhejiang Provincial Natural Science Foundation of China (grant number: LQN26H160018); the China Postdoctoral Science Foundation (Grant Number: 2025M771994).

Author contributions

Hui WANG performed the experimental research and data analysis, wrote and edited the manuscript. Yi LU and Zhongyi LI performed the experimental research and data analysis. Lifeng DING contributed to the study design, data analysis, writing and editing of the manuscript. All authors have read and approved the final manuscript, and therefore, have full access to all the data in the study and take responsibility for the integrity and security of the data.

Compliance with ethics guidelines

Hui WANG, Yi LU, Zhongyi LI and Lifeng DING declare that they have no conflicts of interest.

All animal procedures conformed to the guidelines of Sir Run Run Shaw Hospital, School of Medicine, Zhejiang University. The animal's study protocol was approved by the Ethics Committee of Sir Run Run Shaw Hospital, School of Medicine, Zhejiang University (Approval number: SRRSH20250905).

Declaration on the use of generative AI tools

During the preparation of this work, the authors used ChatGPT to improve language and readability. After using this tool, the authors reviewed and edited the content as needed and take full responsibility for the content of the publication.

References

Bai J, Zhang X, Meng W, Xu H, Liu Y, Zhong Y, Lin X, Wang J, Fan D, Lv G, Gu Y. 2024. Dioscin decreases M2 polarization via inhibiting a positive feedback loop between RBM47 and NF-κB in glioma. Phytomedicine. 128:155417. https://doi.org/10.1016/j.phymed.2024.155417

Bex A, Ghanem YA, Albiges L, Bonn S, Campi R, Capitanio U, Dabestani S, Hora M, Klatte T, Kuusk T, et al. 2025. European Association of Urology Guidelines on Renal Cell Carcinoma: The 2025 Update. Eur Urol. 87(6):683–696. https://doi.org/10.1016/j.eururo.2025.02.020

Chen Y-W, Wang L, Panian J, Dhanji S, Derweesh I, Rose B, Bagrodia A, McKay RR. 2023. Treatment Landscape of Renal Cell Carcinoma. Curr Treat Options Oncol. 24(12):1889–1916. https://doi.org/10.1007/s11864-023-01161-5

Er-Rahmani S, Errabiti B, Matencio A, Trotta F, Latrache H, Koraichi SI, Elabed S. 2024. Plant-derived bioactive compounds for the inhibition of biofilm formation: a comprehensive review. Environ Sci Pollut Res Int. 31(24):34859–34880. https://doi.org/10.1007/s11356-024-33532-2

Gao H, Wang Z, Zhu D, Zhao L, Xiao W. 2024. Dioscin: Therapeutic potential for diabetes and complications. Biomed Pharmacother. 170:116051. https://doi.org/10.1016/j.biopha.2023.116051

George Warren W, Osborn M, Yates A, Wright K, O'Sullivan SE. 2023. The emerging role of fatty acid binding protein 5 (FABP5)

in cancers. Drug Discov Today. 28(7):103628. https://doi.org/10.1016/j.drudis.2023.103628
Hao S, Yang H, Hu J, Luo L, Yuan Y, Liu L. 2024. Bioactive compounds and biological functions of medicinal plant-derived extracellular vesicles. Pharmacol Res. 200:107062. https://doi.org/10.1016/j.phrs.2024.107062
Ivanyi P, Fröhlich T, Grünwald V, Zschäbitz S, Bedke J, Doehn C. 2024. The Treatment of Metastatic Renal Cell Carcinoma. Dtsch Arztebl Int. 121(17):576–586. https://doi.org/10.3238/arztebl.m2024.0147
Jin J, Xie Y, Zhang J-S, Wang J-Q, Dai S-J, He W-F, Li S-Y, Ashby CR, Chen Z-S, He Q. 2023. Sunitinib resistance in renal cell carcinoma: From molecular mechanisms to predictive biomarkers. Drug Resist Updat. 67:100929. https://doi.org/10.1016/j.drup.2023.100929
Kou F, Li X-Y, Feng Z, Hua J, Wu X, Gao H, Lin J, Kang D, Li A, Li J, et al. 2025. GPR171 restrains intestinal inflammation by suppressing FABP5-mediated Th17 cell differentiation and lipid metabo-lism. Gut. 74(8):1279–1292. https://doi.org/10.1136/gutjnl-2024-334010
Kou Y, Zhu R, Gu F, Tang H, Yang R, Wang Yuqing, Wang Yunshuai, Han B. 2026. Dioscin suppresses epithelial-mesenchymal transition in gastric cancer by upregulating Cx43 to inhibit the VEG-FA/PI3K/Akt/mTOR pathway. Phytomedicine. 150:157646. https://doi.org/10.1016/j.phymed.2025.157646
Lai Y, Peng Z, He Z, Lu Z, Yan S, Nie Q, Xiang Y. 2025. Dioscin initiates dual roles in bladder cancer progression via miR-195-5p/FASN/SLC3A2 axis-mediated cell death mechanisms. Transl Oncol. 61:102534. https://doi.org/10.1016/j.tranon.2025.102534
Li D, Duan H, Jiang Z, Zhou C, Cao C, Ni M, He L, Zhu X, Jin L, Liu W, et al. 2025. Oxidative stress-induced decreased expression of FABP5 leads to mitochondrial damage and survival disorder of decidual stromal cells in women with recurrent spontaneous abortion. Free Radic Biol Med. 237:270–284. https://doi.org/10.1016/j.freeradbiomed.2025.06.003
Li M, Wang X, Guo J, Qu J, Cao Y, Song Q, Lu J. 2025. Effects of FABP5 Expression on Clinico-pathological and Survival Characteristics in Digestive System Malignancies: A Systematic Review and Meta-Analysis. Cancer Med. 14(7):e70794. https://doi.org/10.1002/cam4.70794
Pham D-X, Hsu T. 2025. Tumor-initiating and metastasis-initiating cells of clear-cell renal cell car-cinoma. J Biomed Sci. 32(1):17. https://doi.org/10.1186/s12929-024-01111-9
Rose TL, Kim WY. 2024. Renal Cell Carcinoma: A Review. JAMA. 332(12):1001–1010. https://doi.org/10.1001/jama.2024.12848
Song M, Zhu X, Zhao X, Feng J, Sui X. 2026. Plant-Derived Bioactive Compounds in Inflamma-tion-Related Cancers: Mechanisms and Therapeutic Potential. Plants (Basel). 15(4). https://doi.org/10.3390/plants15040575
Wang M, Zhang Y, Ni S, Sun M, Wu Q, Wu X, Chen Q, Wang S. 2025. The anti-cancer activity of Dioscin: an update and future perspective. Med Oncol. 42(3):63. https://doi.org/10.1007/s12032-024-02572-6
Wang R, Li X, Gan Y, Liao J, Han S, Li W, Deng G. 2024. Dioscin inhibits non-small cell lung cancer cells and activates apoptosis by downregulation of Survivin. J Cancer. 15(5):1366–1377. https://doi.org/10.7150/jca.89831
Wu L, Ou G-L, Zhang W, Ma H-X, Li X-Y, Zhen Y-H, Wu H, Cao K, Li H-Y. 2025. Fatty acid-binding proteins in cancers. Int J Surg. 111(11):8402–8422. https://doi.org/10.1097/JS9.0000000000003049
Yu Y-Y, Feng M, Chen Y, Jia H-L, Zhang Q, Tong M, Li Y-X, Zhao Y, Liu X-X, Cao S-F, et al. 2025. Asprosin-FABP5 Interaction Modulates Mitochondrial Fatty Acid Oxidation through PPARα Con-tributing to MASLD Development. Adv Sci (Weinh). 12(21):e2415846. https://doi.org/10.1002/advs.202415846

Supplementary information

Materials and methods; Tables S1 and S2; Figs. S1-S3